Supplementary Materials

S1 Dataset

The P (precipitation), Ep (potential evapotranspiration), soil moisture and runoff datasets are all integrated into this analysis. CMIP6 model projections (https://cds.climate.copernicus.eu/datasets/projections-cmip6?tab=download) under the different shared socioeconomic pathways (SSPs) are taken as future simulations. The changes in dryness and wetness are analyzed using these datasets, along with the land water balance and hydroclimatic regimes. Our approach improves the ability to reproduce regional variations in hydrological responses to climatic shifts by accounting for multiple variables, such as soil moisture and runoff.

Table S1: List of GCMs used under SSPs (245 and 585)

Model Name	Institution	Horizontal Resolution	**245**	**585**
ACCESS-CM2	Australian Community Climate and Earth-System Simulator (ACCESS)	1.25° latitude × 1.875° longitude	✓	✓
CMCC-ESM2	Centro Euro-Mediterraneo sui Cambiamenti Climatici (CMCC), Italy	0.75° × 0.75°	✓	✓
CanESM5	Canadian Centre for Climate Modelling and Analysis (CCCma), Environment and Climate Change Canada	Atmosphere: ~2.8° (T63 spectral resolution); Ocean: ~1°	✓	✓
CMCC-CM2-SR5	CMCC/Italy	1.25°x0.9375°	✓	✓
FGOALS-f3-L	Chinese Academy of Sciences (CAS), China	Atmosphere: ~1° (384 × 192 longitude/latitude); Ocean: ~1°	✓	✓
MIROC6	Japan Agency for Marine-Earth Science and Technology (JAMSTEC), Atmosphere and Ocean Research Institute (AORI) of the University of Tokyo, and National Institute for Environmental Studies (NIES), Japan	Atmosphere: ~1.4° (T85 spectral resolution); Ocean: ~1°	✓	✓
GFDL-ESM4	NOAA-GFDL/USA	1°x1.25°	✓	✓

S2 Results

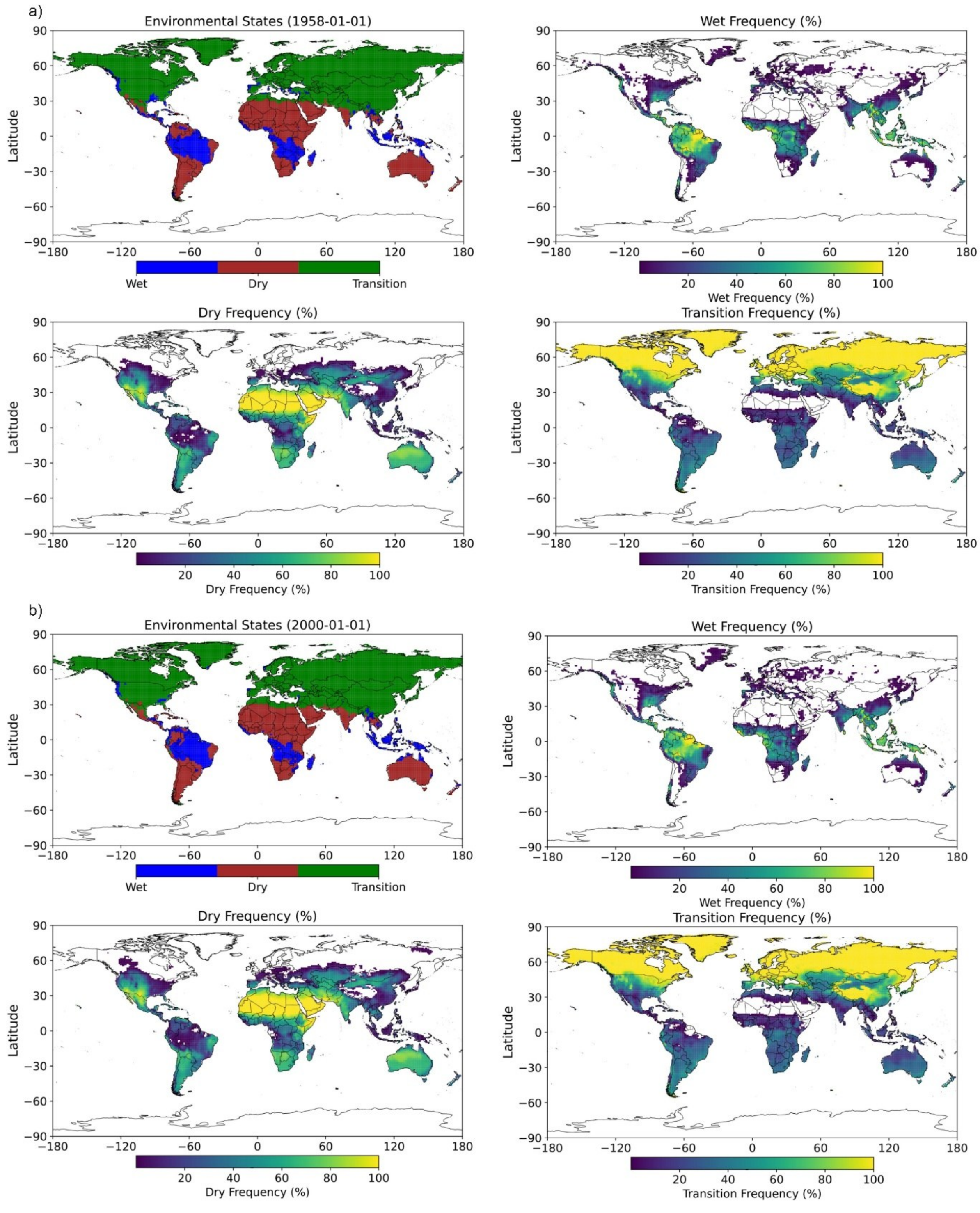

Fig. S1: a) Spatial distribution and frequency analysis of environmental states (1958–2000). The environmental states are derived from precipitation, soil moisture, and potential evaporation. Three panels depict the frequency of each state over the entire period in percentage: Dry Frequency (%), Wet Frequency (%), and Transition Frequency (%). .b) Spatial distribution and frequency analysis of environmental states (2000–2023). The environmental states are derived from precipitation, soil moisture, and potential evaporation. Three panels display the frequency of each state over the entire period in percentages: Dry Frequency (%), Wet Frequency (%), and Transition Frequency (%).

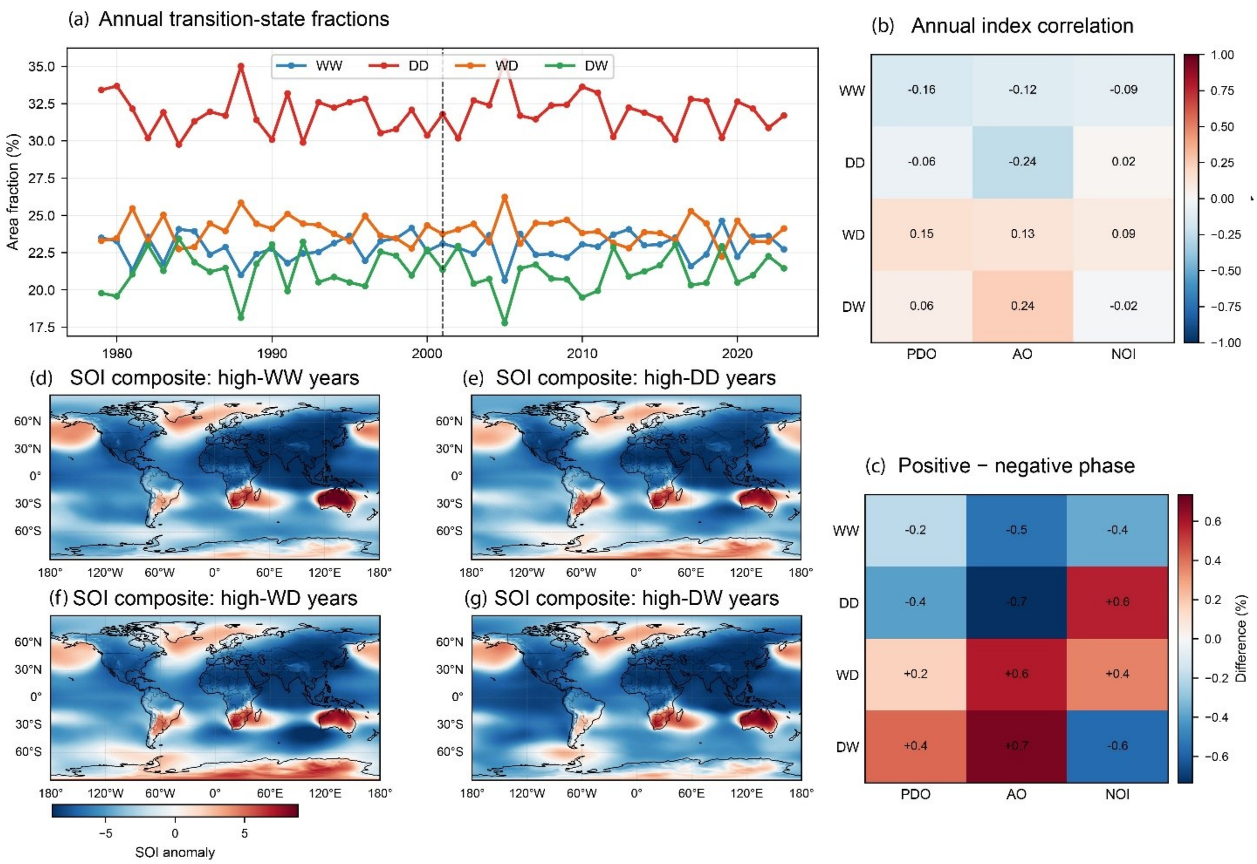

Fig. S2: Large-scale climate associations with SPEI wetting, drying, and transition states. (a) Annual global area fractions of WW, DD, WD, and DW. The vertical dashed line marks the division between the two analysis periods; (b) Annual correlations between transition-state fractions and the selected climate indices (PDO, AO, and NOI); (c) Differences in transition-state fractions between positive and negative phases of each index. Positive values indicate larger fractions during the positive phase, whereas negative values indicate larger fractions during the negative phase; (d–g) Spatial composites of gridded SOI during years with high global fractions of WW, DD, WD, and DW, respectively. The SOI composites provide diagnostic large-scale climate context and support physical interpretation, but they do not constitute formal causal attribution.

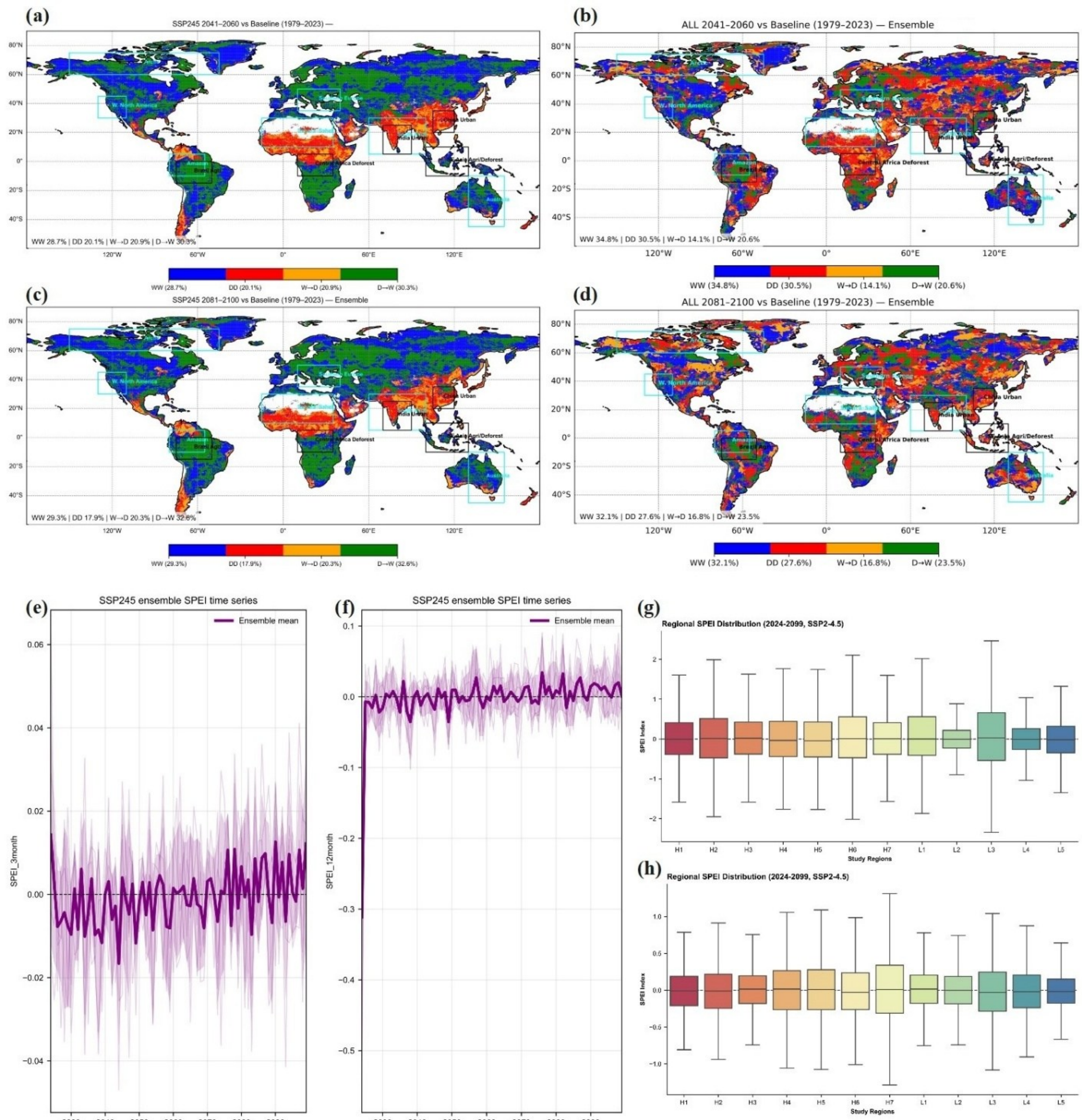

Fig. S3: Future hydroclimatic transition states under SSP245 across short （3-month） and long (12-month) SPEI timescales. The ensemble transition states for SPEI-3 and SPEI-12 during 2041–2060 and 2081–2100, compared to the 1979–2023 baseline. WW indicates wet-to-wet persistence, DD dry-to-dry persistence, WD wet-to-dry transition, and DW dry-to-wet transition. Insets display the ensemble mean SPEI time series, while box plots depict regional SPEI distributions in selected hotspot and lower-signal regions.

S2.2 WW-DD paradigm based on precipitation and potential evaporation anomalies

Kernel density estimation (KDE) was applied to smooth the evaporation (ΔE) and precipitation (ΔP) anomalies across six major river basins (e.g., Amazon, Yangtze, Ganges, Nile, Mississippi, and Murray-Darling) to visualize the predominant transitions for each basin under SSP245 and SSP585 (Figure S4 and S5). Each subplot for the six basins displays the transitions between historical and future periods. Scatter points represent transitions, and the KDE contours in the background represent areas of high density. The density contours show the transitions (where most data points and changes occur). The projections reveal critical differences in the basin-specific responses to climate change, including increased variability, intensified drought, and changes in wetting patterns.

Under higher emissions, the increases in "WD" transitions shown by the SSP585 scenario are less frequent than those in SSP245 but are sharper in the 2061–2099 period in the Amazon Basin. In both scenarios, "WW" transitions persist, but their density decreases for SSP585 because of weakening rainforest resilience. These results are consistent with studies documenting the vulnerability of the Amazon to tipping points under increasingly warm and deforestation pressures (Zemp et al., 2017). The SSP245 scenario depicts a less extreme change with more balanced trends of drying and wetness and, hence, partial resilience under moderate emissions.

Both scenarios are also markedly different for the Yangtze Basin. The density of "WD" transitions explodes under SSP585 (particularly for 2061–2099), signifying heightened flood and drought variability. However, we also see such 'DW' transitions with reduced density, which indicates the weakening of compensatory wetting effects under extreme warming. For example, SSP245 has more balanced transitions that consist of patterns of both drying and wetting but that occur over different timescales across both periods. Previous studies conducted by (Qiu and Zhou, 2019; Wu et al., 2016) have shown that the Yangtze River Basin is sensitive to a warming world in a way that correlates with a broader range of intensified monsoon variability. Both periods are controlled by severe reductions in monsoon precipitation and increasing drought risk in SSP585 projections, which are overwhelmingly dominated by 'WD' transitions in the Ganges Basin. SSP245 presents WD transitions with lower intensity and density and likely represents some degree of monsoon preservation under moderate emissions. These results are consistent with those of (Paul et al., 2016; Rao et al., 1996; Roxy et al., 2017), who pointed to a modest weakening in precipitation trends. However, the SSP585 projections to 2050 exacerbate the agricultural and socioeconomic vulnerabilities in the Ganges Basin and raise concerns about water security (Banerjee and Pandey, 2021; Das et al., 2021). Under SSP585, the Nile River Basin shifts to more 'DD' transitions, indicating continuing aridity and a long-term decline in water availability for the latter period. "DW" transitions are observed with lower density than SSP245 transitions because of increased variability and a stronger drying signal. In contrast, SSP245 closely matches the result of a wholly fixed 'default' simulation with higher density transitions in the 'DW' zones; this may indicate that, in some regions, 'DW' transitions can occur under moderate emissions. (Melesse and Demissie, 2024) reviewed the Nile River's sensitivity to upstream water management and climate variability, with SSP585 experiencing increasingly arid conditions. For the Mississippi Basin, the SSP585 projections produced a clear dominance of "DD" transitions, especially in the latter period, due to the increased risk of droughts over the central US. The results show that drying transitions are significantly denser under high-emissions SSP585 than under near-current-emissions SSP245, implying more severe impacts under high-emissions scenarios. (Cook et al., 2015) highlighted that warming scenarios increase drought risk and severe consequences, especially under SSP585. For SSP585, the Murray–Darling Basin exhibited persistent 'DD' transitions with higher density than

SSP245. This is in line with the findings of (Collins et al., 2022; Devanand et al., 2024), who reported arid conditions in southeastern Australia due to extreme warming. Although SSP245 also has drying trends, there are fewer 'DD' transitions, suggesting a lower impact from moderately emitting climates. This comparison highlights the critical need for emission mitigation to preserve water availability in this vulnerable basin.

SSP585 consistently exhibited stronger drying trends throughout all the basins, with intense 'WD > DD' transitions prevalent within the Amazon, Ganges, and Mississippi River Basins. On the other hand, SSP245 shows more balanced transitions, with some wetting patterns retained in the Amazon, Yangtze, and Nile River Basins. These results highlight the critical importance of emission reductions in alleviating severe water stress and maintaining basin resilience under future climate scenarios. These emission pathways present divergent challenges for effective water management and adaptation strategies.

SSP 245

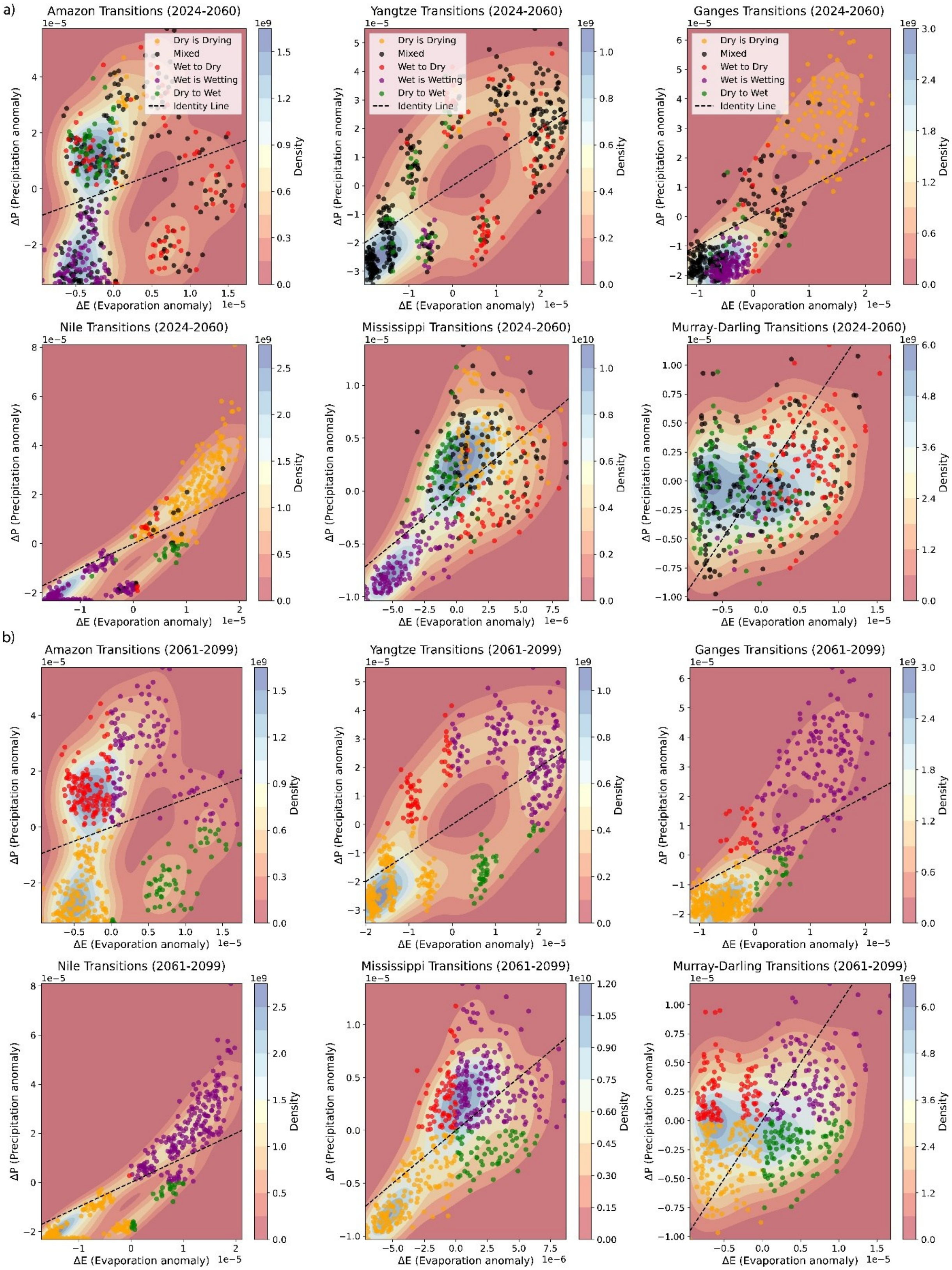

Dry is Drying (DD); Wet is wetting (WW); Dry to Wet (DW); Wet to Dry (WD)

Fig. S4: Transition dynamics in evaporation (ΔE) and precipitation (ΔP) anomalies for six major river basins (Amazon, Yangtze, Ganges, Nile, Mississippi, and Murray-Darling) during (a) 2024–2060 and (b) 2061-20299 under the SSP245 scenario. Scatter points represent categorized transitions: "Dry is Drying (DD)," "Wet to Dry (WD)," "Dry to Wet (DW)," "Wet is Wetting (WW)," and "Mixed," with density contours highlighting regions of concentrated transitions. The identity line (dashed) indicates no change in conditions

SSP 585

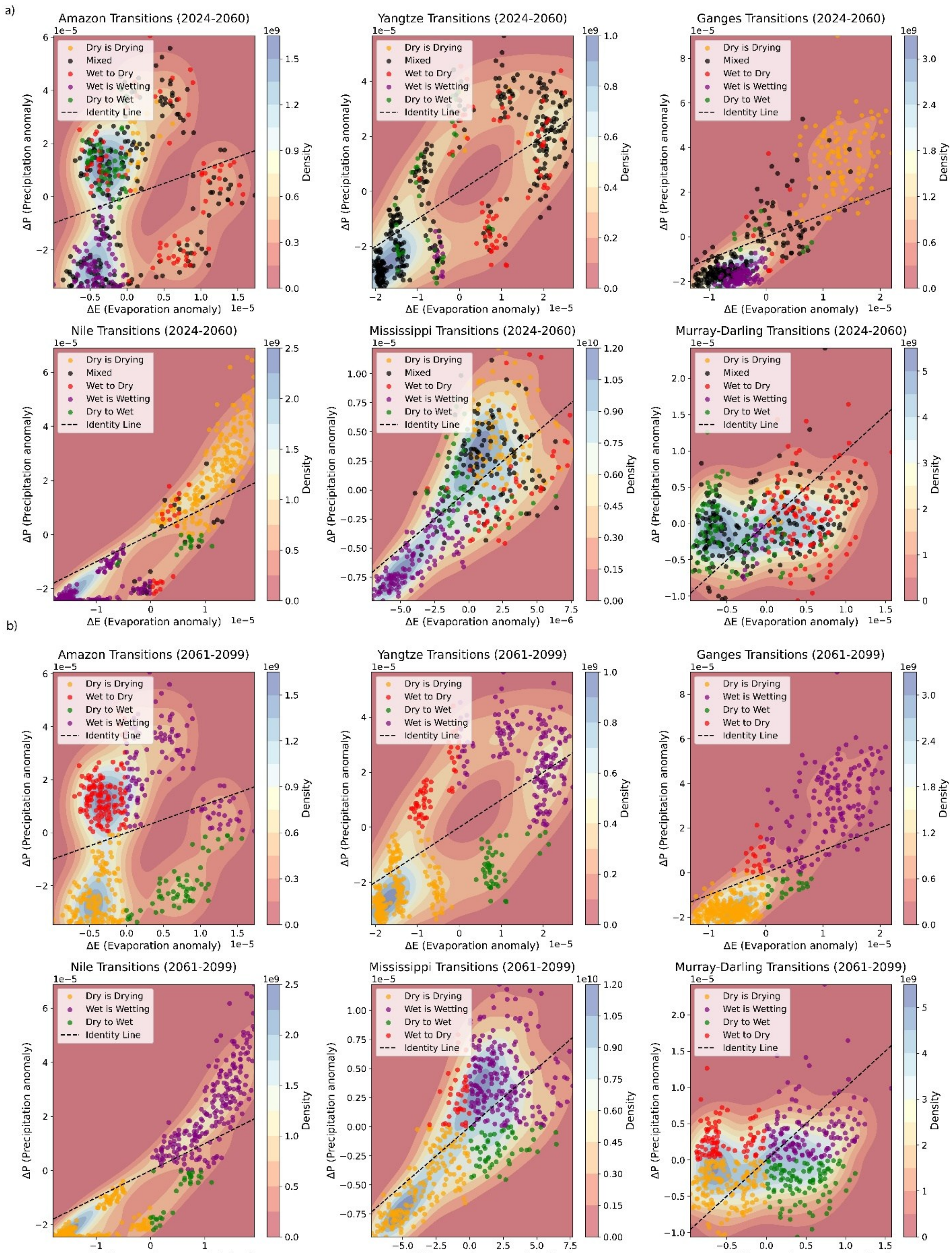

Dry is Drying (DD); Wet is wetting (WW); Dry to Wet (DW); Wet to Dry (WD)

Fig. S5: Transition dynamics in evaporation (ΔE) and precipitation (ΔP) anomalies for six major river basins (Amazon, Yangtze, Ganges, Nile, Mississippi, and Murray-Darling) during (a) 2024–2060 and (b) 2061-20299 under the SSP585 scenario. Scatter points represent categorized transitions: "Dry is Drying (DD)," "Wet to Dry (WD)," "Dry to Wet (DW)," "Wet is Wetting (WW)," and "Mixed," with density contours highlighting regions of concentrated transitions. The identity line (dashed) indicates no change in conditions.

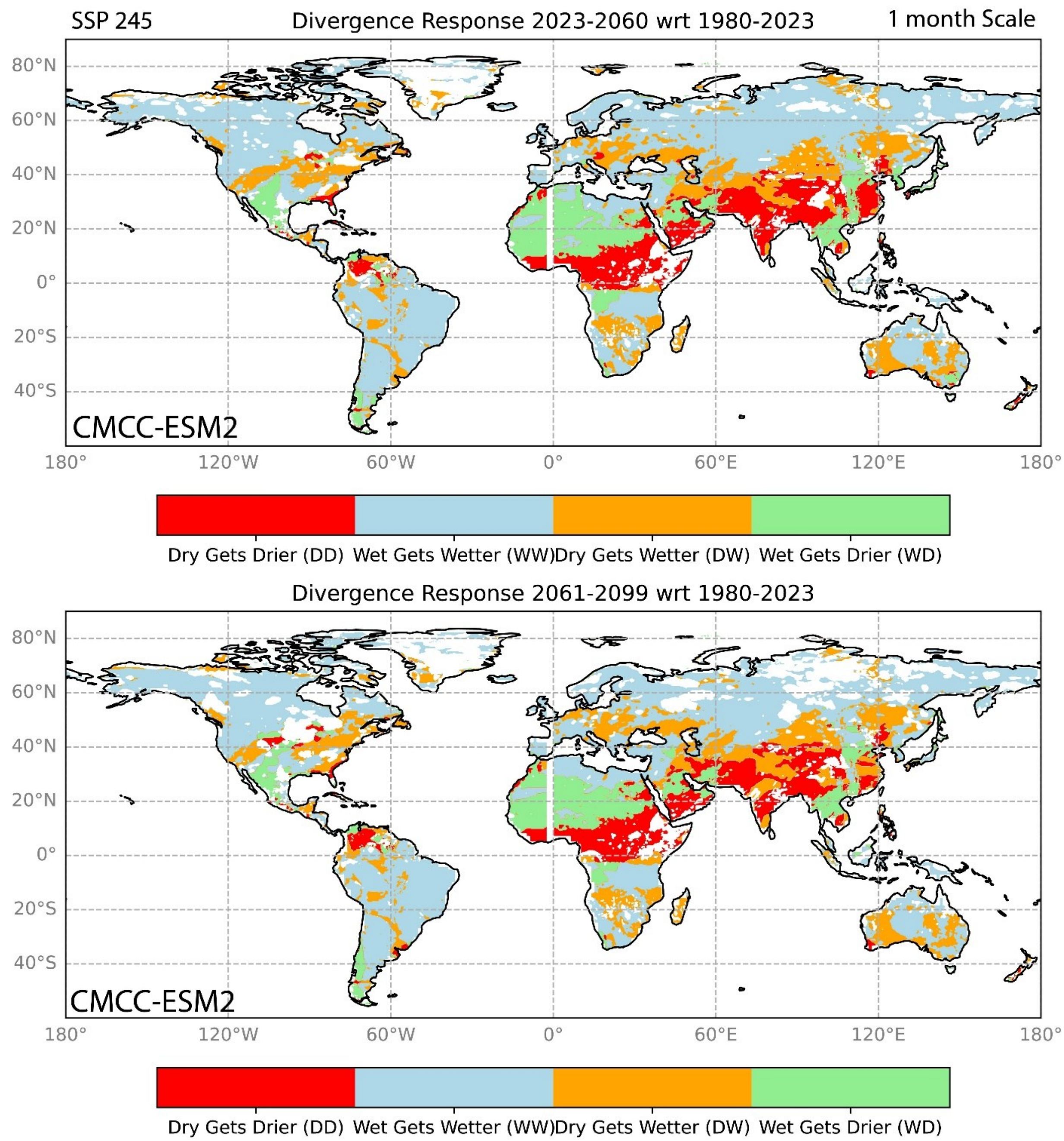

Fig. S6: Future divergence computation based on SPEI using modeled water balance at a monthly scale under SSP 245 CMCC-ESM2model (listed in supplementary material) from 1981-2023 to 2023-2060 and 2061-2099. The Wet Gets Wetter category is calculated when historical and future trends are positive (divergence). Dry Gets Drier: when both historical and future trends are negative (divergence). Transition Wet to Drier occurs when the historical trend is positive (non-divergence), and the future trend is negative. Dry to wetter when the historical trend is negative, and the future trend is positive (non-divergence). The percentage is the area under each category.

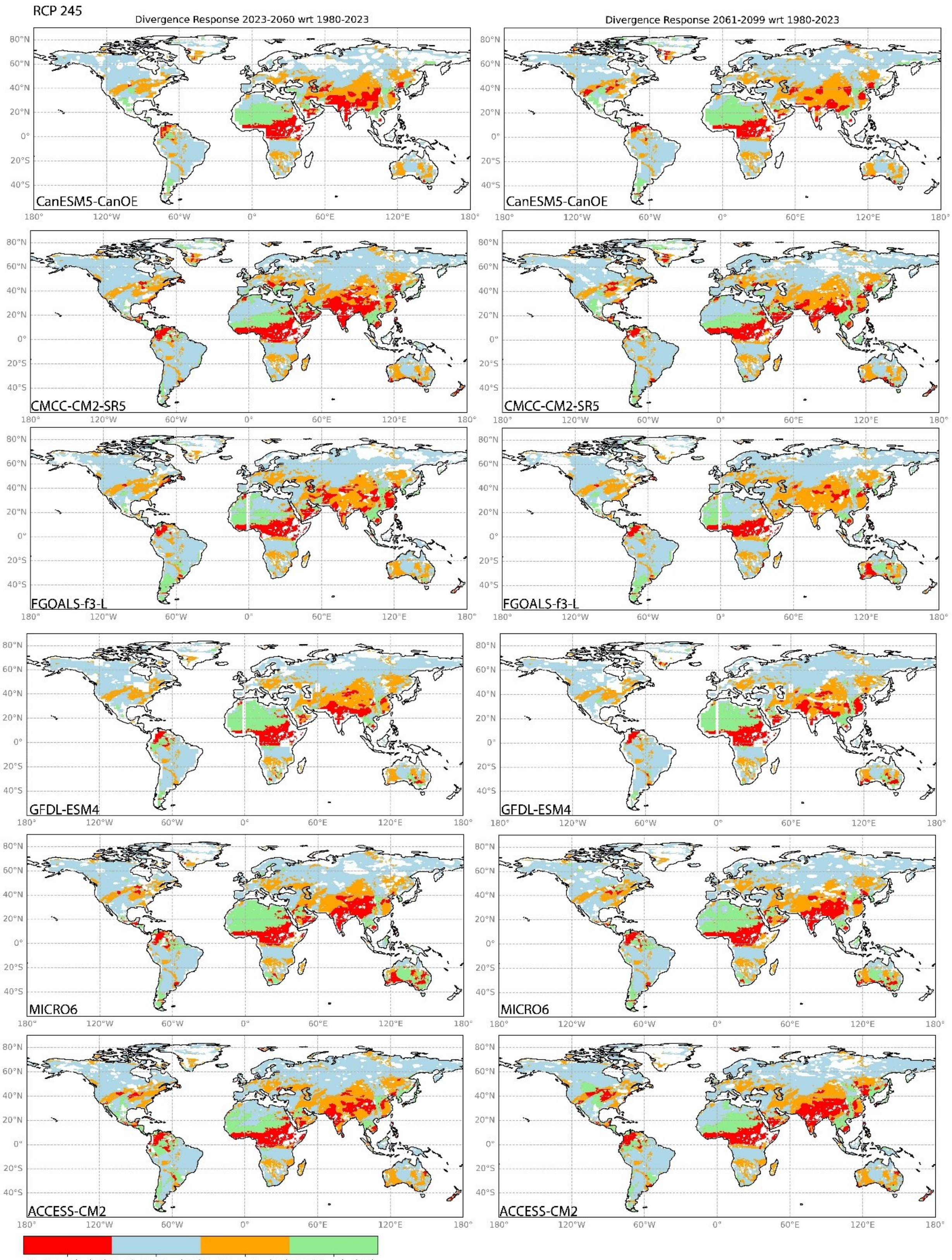
RCP 245
Divergence Response 2023-2060 wrt 1980-2023
Divergence Response 2061-2099 wrt 1980-2023
CanESM5-CanOE
CMCC-CM2-SR5
FGOALS-f3-L
GFDL-ESM4
MICRO6
ACCESS-CM2
Dry Gets Drier (DD)
Wet Gets Wetter (WW)
Dry Gets Wetter (DW)
Wet Gets Drier (WD)

Fig. 7: Future divergence computations based on the SPEI using the modeled water balance at a monthly scale under different SSP 245 models (listed in the supplementary material) from 1981-2023 to 2023-2060 and 2061-2099. The wet gets wetter category is calculated when the historical and future trends are positive (divergence). Dry gets drier occurs when both the historical and future trends are negative (divergence). The transition from wet to drier occurs when the historical trend is positive (nondivergence) and the future trend is negative. A dry to wetter trend is indicated when the historical trend is negative, and the future trend is positive (nondivergence). The percentage is the area under each category.

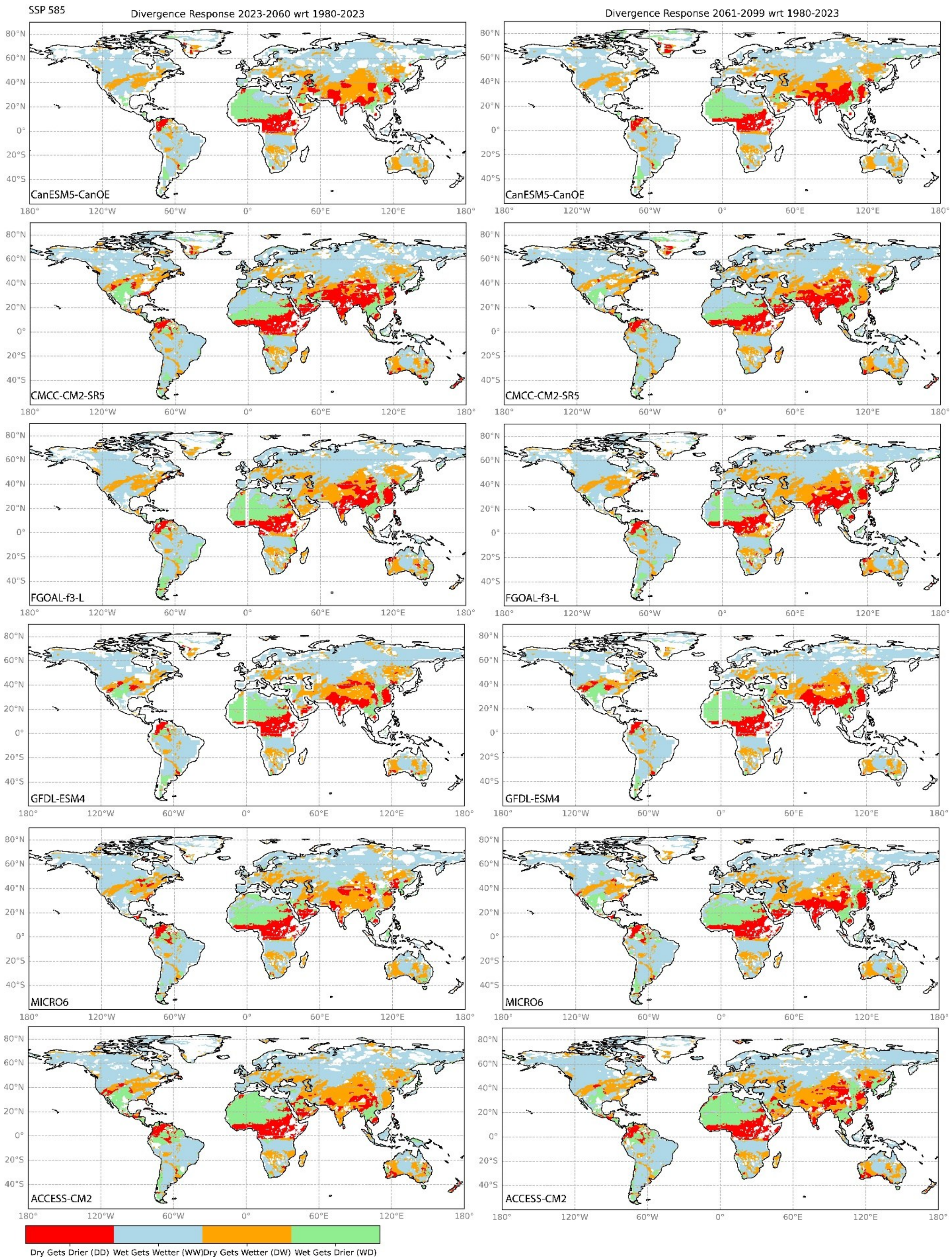

SSP 585
Divergence Response 2023-2060 wrt 1980-2023
Divergence Response 2061-2099 wrt 1980-2023
CanESM5-CanOE
CMCC-CM2-SR5
FGOAL-f3-L
GFDL-ESM4
MICRO6
ACCESS-CM2
Dry Gets Drier (DD)
Wet Gets Wetter (WW)
Dry Gets Wetter (DW)
Wet Gets Drier (WD)

Fig. S8: Future divergence computation based on SPEI using the modeled water balance at 12 month scale under different SSP 585 models (listed in supplementary material) from 1981-2023 to 2023-2060 and 2061-2099. The Wet Gets Wetter category is calculated when historical and future trends are positive (divergence). Dry Gets Drier: when both historical and future trends are negative (divergence). Transition Wet to Drier occurs when the historical trend is positive (non-divergence), and the future trend is negative. Dry to wetter when the historical trend is negative, and the future trend is positive (non-divergence). The percentage is the area under each category.

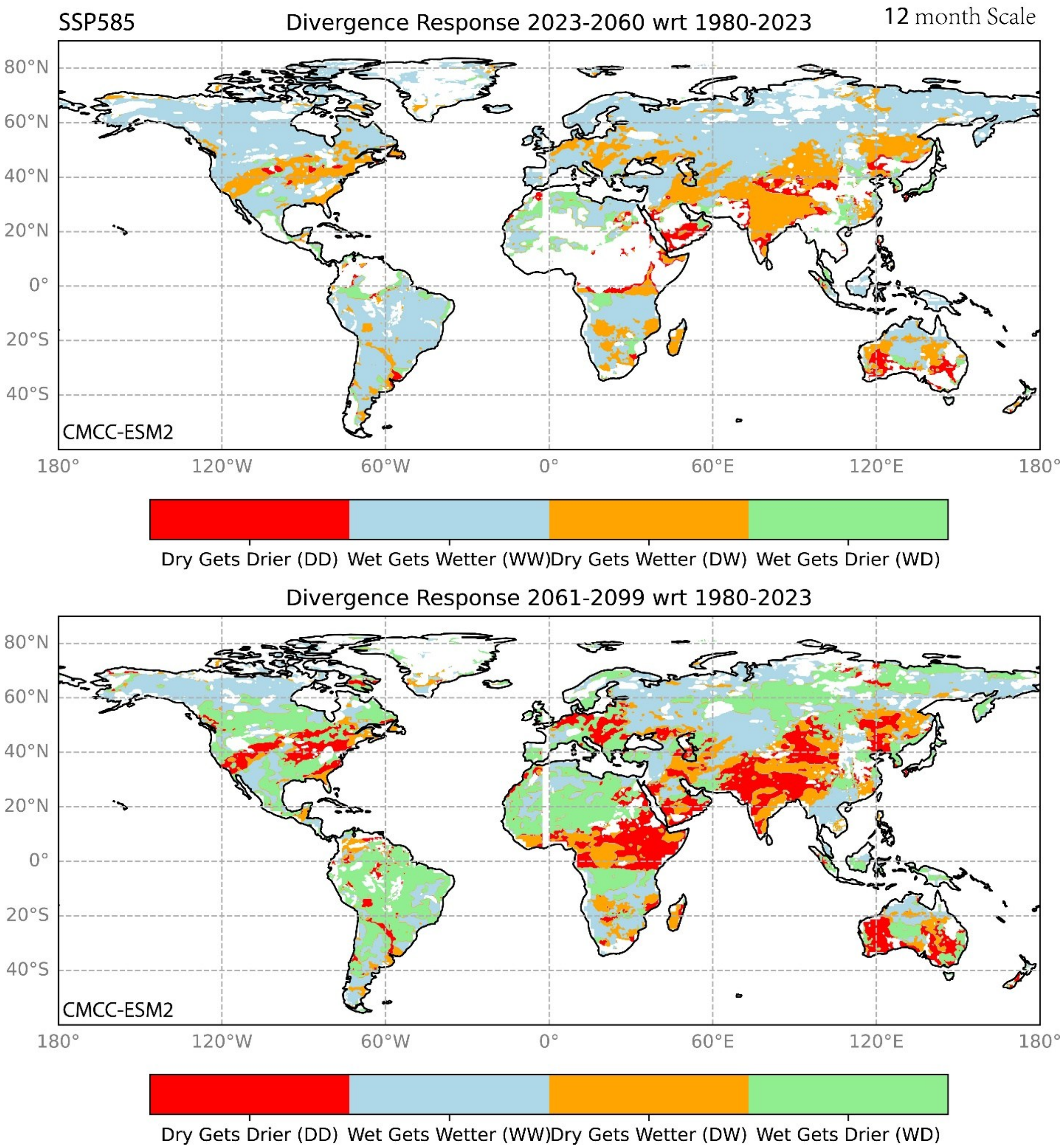

Fig. S9: Future divergence computation based on SPEI using the modeled water balance at a monthly scale under SSP 585 CMCC-ESM2model (listed in supplementary material) from 1981-2023 to 2023-2060 and 2061-2099. The Wet Gets Wetter category is calculated when historical and future trends are positive (divergence). Dry Gets Drier: when both historical and future trends are negative (divergence). Transition Wet to Drier occurs when the historical trend is positive (non-divergence), and the future trend is negative. Dry to wetter when the historical trend is negative, and the future trend is positive (non-divergence). The percentage is the area under each category.

References

Banerjee, S., Pandey, A.C., 2021. Catchment-level agricultural drought hazard vulnerability analysis of Ganga Basin (India) using spectral indices. Arab J Geosci 14, 1782. https://doi.org/10.1007/s12517-021-07825-6

Collins, L., Clarke, H., Clarke, M.F., McColl Gausden, S.C., Nolan, R.H., Penman, T., Bradstock, R., 2022. Warmer and drier conditions have increased the potential for large and severe fire seasons across south-eastern Australia. Global Ecol Biogeogr 31, 1933–1948. https://doi.org/10.1111/geb.13514

Cook, B.I., Ault, T.R., Smerdon, J.E., 2015. Unprecedented 21st century drought risk in the American Southwest and Central Plains. Sci. Adv. 1, e1400082. https://doi.org/10.1126/sciadv.1400082

Das, S., Hazra, S., Haque, A., Rahman, M., Nicholls, R.J., Ghosh, A., Ghosh, T., Salehin, M., De Campos, R.S., 2021. Social vulnerability to environmental hazards in the Ganges-Brahmaputra-Meghna delta, India and Bangladesh. International Journal of Disaster Risk Reduction 53, 101983.

Devanand, A., Falster, G.M., Gillett, Z.E., Hobeichi, S., Holgate, C.M., Jin, C., Mu, M., Parker, T., Rifai, S.W., Rome, K.S., Stojanovic, M., Vogel, E., Abram, N.J., Abramowitz, G., Coats, S., Evans, J.P., Gallant, A.J.E., Pitman, A.J., Power, S.B., Rauniyar, S.P., Taschetto, A.S., Ukkola, A.M., 2024. Australia's Tinderbox Drought: An extreme natural event likely worsened by human-caused climate change. Sci. Adv. 10, eadj3460. https://doi.org/10.1126/sciadv.adj3460

Melesse, M.B., Demissie, Y., 2024. Hydrology and Droughts in the Nile: A Review of Key Findings and Implications. Water 16, 2521.

Paul, S., Ghosh, S., Oglesby, R., Pathak, A., Chandrasekharan, A., Ramsankaran, R., 2016. Weakening of Indian summer monsoon rainfall due to changes in land use land cover. Scientific reports 6, 32177.

Qiu, S., Zhou, W., 2019. Variation in summer rainfall over the Yangtze River region during warming and hiatus periods. Atmosphere 10, 173.

Rao, P.G., Kelly, P.M., Hulme, M., 1996. Recent climatic change, greenhouse gas emissions and future climate: The implications for India. Theor Appl Climatol 55, 41–64. https://doi.org/10.1007/BF00864702

Roxy, M.K., Ghosh, S., Pathak, A., Athulya, R., Mujumdar, M., Murtugudde, R., Terray, P., Rajeevan, M., 2017. A threefold rise in widespread extreme rain events over central India. Nature communications 8, 1–11.

Wu, Y., Wu, S.-Y., Wen, J., Tagle, F., Xu, M., Tan, J., 2016. Future changes in mean and extreme monsoon precipitation in the middle and lower Yangtze River Basin, China, in the CMIP5 models. Journal of Hydrometeorology 17, 2785–2797.
Zemp, D.C., Schleussner, C.-F., Barbosa, H.M., Hirota, M., Montade, V., Sampaio, G., Staal, A., Wang-Erlandsson, L., Rammig, A., 2017. Self-amplified Amazon forest loss due to vegetation-atmosphere feedbacks. Nature communications 8, 14681.